18th International Conference on Space Operations, Montreal, Canada, 26 - 30 May 2025.

SpaceOps-2025, ID # 482

NEOSSat's Extended Mission: Assessing the Operational Impact of Battery Degradation

Marc-Antoine Lavoie[a]

[a] *Calian Advanced Technologies, Canadian Space Agency, 6767 route de l'Aéroport, Saint-Hubert, Québec, J3Y 8Y9, Canada. marc-antoine.lavoie@calian.com*

Abstract

The Near-Earth Object Surveillance Satellite (NEOSSat) is a Canadian space telescope orbiting the Earth in a sun-synchronous orbit. Its orbital configuration entails an annual 100-day eclipse season, peaking around the winter solstice and during which the satellite enters Earth's shadow for up to 22 minutes each orbit, relying solely on its battery for power supply. Now in its 13th year of operation, well beyond the 2-year design life, NEOSSat has experienced both performance degradation and failures across several onboard systems. Nevertheless, science operations have been sustained through operational workarounds and innovative flight software updates. This paper examines the degradation of its 4.5 Amp-hour lithium-ion battery, with particular emphasis on internal resistance increase and its operational impacts. Recent assessments indicate that the battery still has sufficient capacity to support the spacecraft through eclipses, the only times it is needed as a power source. However, the increase in internal resistance has become problematic. Now at an estimated 2.6 Ω, a 400% increase from the baseline value, it causes significant and hazardous voltage drops on the main power bus. The communications subsystem requires the largest power draw when in use for real-time contacts. With all available ground stations located in the Northern Hemisphere, where eclipse events occur, NEOSSat's battery experiences significant strain during these essential activities. Through the 2021-2022 eclipse season, the onboard power system autonomously triggered a load-shed event during a real-time contact due to a critical voltage drop on the main bus. Investigation identified the root cause as the increased internal resistance of the battery, which rendered voltage readings an unreliable indicator of the battery's state of charge. The onboard load-shed algorithm, limited by hardware-defined voltage thresholds, cannot be adjusted to account for this degradation. In response, the operations team has implemented various strategies to mitigate the risk of undesirable autonomous load-sheds during eclipse seasons. This paper presents the evolution of the estimated internal resistance since the start of the mission, along with projections for future degradation. It outlines the mitigation strategies that have been implemented and discusses planned measures to support continued operations during upcoming eclipse seasons.

Keywords: NEOSSat**, s**atellite operations, lithium-ion batteries, power system management, mission continuity

Nomenclature

Dates are formatted using the year and day of year, e.g., 2024-328, which corresponds to November 23rd, 2024.

Acronyms/Abbreviations

A	Ampere
ADCS	Attitude Determination and Control System
BCR	Battery Charge Regulator
BM	Battery Module
BoL	Beginning of Life
C&DH	Command & Data Handling
CSA	Canadian Space Agency
DCR	Direct Current Resistance
Desat	Dipole Desaturation Mode (attitude control mode for angular momentum dumping)
DLR	Deutsches Zentrum für Luft- und Raumfahrt (German Aerospace Center)
DoD	Depth of Discharge
FSW	Flight Software
GARS	German Antarctic Receiving Station
LS1	Load-Shed level 1
LS2	Load-Shed level 2
LTAN	Local Time of Ascending Node
NEOSSat	Near Earth Object Surveillance Satellite
OCV	Open Circuit Voltage
Ops	Operations
PCDU	Power Control and Distribution Unit
PPT	Power-Point Tracking
S/C	Spacecraft
SHM	Safe Hold Mode
SoC	State of Charge
SPA	Solar Panel
V	Volt

1. INTRODUCTION

The Near-Earth Object Surveillance Satellite (NEOSSat) is Canadian space telescope launched 2013 into a 780 km Sun-synchronous orbit. In over 12 years of operation, NEOSSat has overcome several challenges that could have prematurely ended the mission. Notably, in 2016, the satellite lost both its magnetometer and magnetorquer suite, severely impairing attitude control and forcing an extended suspension of payload operations. Successful recovery efforts restored nominal operations in 2017, and the mission has operated continuously without further disruption ever since. Over the past few years, the operations team has expanded the spacecraft state-of-health monitoring to detect early signs of degradation in onboard units. Recently, the battery system has been the primary focus of these efforts.

NEOSSat's Sun-synchronous orbit results in annual eclipse seasons of approximately 100 days, centered around the winter solstice. During this period, the satellite passes through Earth's shadow on each orbit, with the duration of the eclipse lasting up to 22 minutes. The battery becomes the source of electrical energy when solar power is not available, ensuring continuous operation of the satellite's systems during eclipse periods. This power transfer process had functioned seamlessly until the eclipse season of 2021-2022, when an under-voltage event triggered an autonomous fault response. After a preliminary assessment, it was observed that the battery voltage during eclipses had been dropping progressively each year. The gradual degradation of the battery appears to be the primary cause of this effect.

This study examines NEOSSat's battery degradation and the associated operational impacts. It focuses on the impact of increasing battery internal resistance and summarizes the strategies implemented to mitigate operational disruptions caused by autonomous fault response events. The findings provide insight into how the aging battery system influences the satellite longevity and explore potential approaches to sustaining its operations despite ongoing degradation.

1.1 Orbit Characteristics Evolution

NEOSsat was inserted into a sun-synchronous orbit with a Local Time of Ascending Node (LTAN) of around 06:08. However, since the satellite has no orbit control system, it has no ability to maintain its orbital elements. As a result, the spacecraft's orbit evolves subject to natural perturbations of the Earth's asymmetric gravity, atmospheric drag, solar radiation pressure, and third body perturbations from the Moon and Sun. This will in turn affect the eclipse season parameters over time. The combined effects of those perturbations lead to long-term LTAN oscillations, which directly affects the eclipse lengths and the total span of eclipse seasons. Fig. 1 illustrates the variation of the maximum eclipse duration for each season.

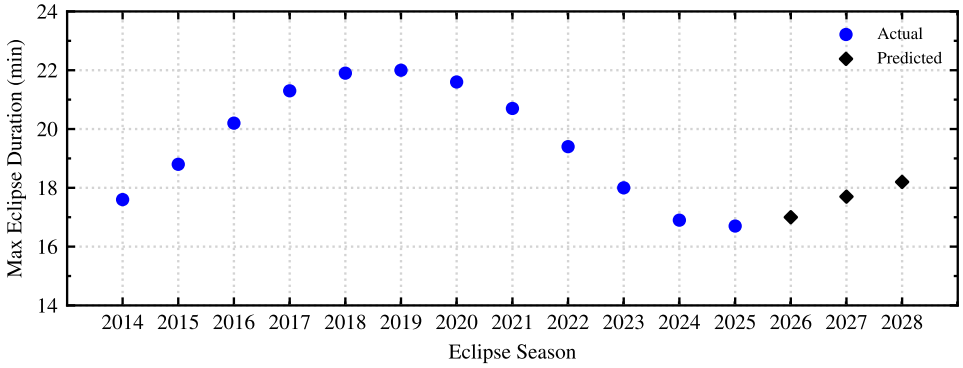

Fig. 1. Maximum eclipse duration evolution since the beginning of the mission

An analysis by the Flight Dynamics group indicates that eclipse season length and eclipse duration reached their minimum in 2025 and will begin increasing again starting in 2026.

1.2 Spacecraft State of Health Overview

Since the beginning of the mission, NEOSSat has experienced three major anomalies, each requiring complex recovery efforts by the operations team. These anomalies have severely impacted the Attitude Determination and

Control System (ADCS), resulting in the complete loss of the magnetometer, all magnetorquers, and the x-axis reaction wheel.

In 2016, the magnetometer failure led to the development of a GPS-based coarse attitude sensing algorithm, repurposing onboard GPS signals for three-axis attitude determination. While this system was being finalized, a microcontroller failure disabled the magnetorquers, requiring the implementation of a new desaturation mode (Desat) using the satellite's residual dipole. This new Desat mode is required for angular momentum dumping between payload activities and it is the new default standby mode. A detailed review of these events can be found in [1]. Lastly, in 2021, the failure of one reaction wheel prompted a swift reconfiguration of the flight software (FSW) to support three-wheel operation.

1.3 Power System Overview

This section reviews important information about the spacecraft's power system specifications and operations. NEOSSat's battery is made of 24 Sony 18650HC cells in an 8s3p configuration: *i.e.* three 8-cell Battery Modules (BM) connected in parallel. Each cell has a nominal capacity of 1.5 Ah and a nominal voltage of 4.2 V, for a total capacity of 4.5 Ah (3 × 1.5 Ah) and a nominal full charge voltage of 33.6 V (8 × 4.2 V). The main battery specifications are summarized in Table 1. Note that these values correspond to Beginning of Life (BoL) conditions.

Table 1. Battery BoL specifications

Cells		**Battery**		
Capacity:	1.5 Ah	Capacity (C):	4.5 Ah	
Full Charge Voltage:	4.2 V	Full Charge Voltage:	33.6 V	(100% SoC)
Overvoltage Protection:	4.5 V	Full Discharge Voltage:	24.0 V	(0% SoC)
Nominal Ops Temperature:	10 - 40 °C			

1.3.1 Power Control and Distribution Unit (PCDU) Characteristics and Telemetry Data

Fig. 2 below shows a simplified block diagram of the main power system components. Each battery module is modelled with simple voltage sources (ε) in series with resistors (R_i). Electromagnetic radiation from the Sun is converted into electrical energy by the seven Solar Panels (SPA), which are controlled by Power-Point Tracking circuits (PPT) to provide a regulated energy source for the battery and the rest of NEOSSat's equipment. The reaction wheels can also transfer their kinetic energy back into the battery when slowing down, acting as a second source of electrical energy from the battery point of view.

The two primary measurements for analysing energy flow are the battery terminal voltage and current. These are provided as telemetry points with a sampling period of 14.4 seconds. The battery follows the voltage source convention, where positive current flows out of the positive terminal. As a result, battery current readings are negative during charging and positive during discharging. These measurements will be used to estimate other electrical properties, such as power, energy, resistance, and capacity. Note that there is no onboard State of Charge (SoC) estimation available.

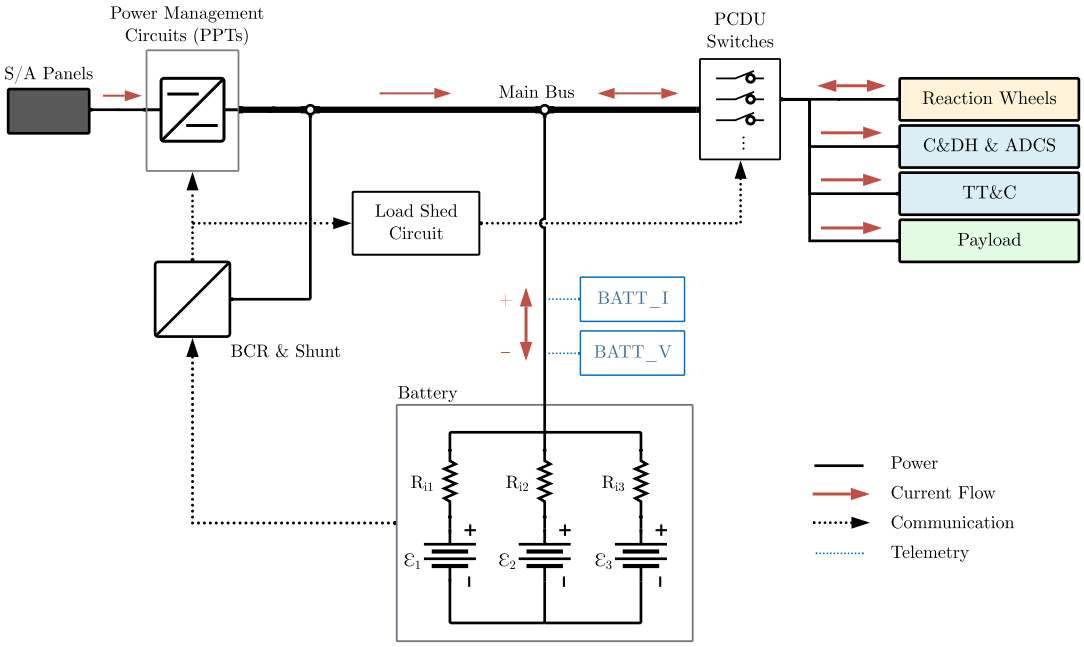

Fig. 2. NEOSSat simplified power system diagram

The battery charge rate is set by the SPA controllers and must remain below 2.25 A under all operational conditions, in accordance with the manufacturer's recommendations. The battery and main bus maximum operating voltage is controlled by the Battery Charge Regulators (BCR) and the shunt regulator. The BCR limits the amount of harvested energy from the PPT circuits when the battery voltage reaches 33.6 V by backing off the PPT from their maximum operating power point, effectively switching the charging mode from constant current to constant voltage. To avoid overcharging, the shunt regulator dissipates any excessive energy as heat when the battery is fully charged.

1.3.2 Autonomous Load-Shedding

Load-shed protocols onboard satellites are essential for maintaining critical functions during power shortages. They prioritize vital subsystems while shutting down or reducing power to non-essential components. NEOSSat's load-shed strategy is based on a dedicated monitoring circuit, which uses resistive voltage dividers and simple comparators to detect and react to under-voltage conditions. This hardware approach is thus fully independent of the onboard Flight Software (FSW). Only a load-shed flag signal can be detected by the FSW when a load-shed condition occurs. The reaction to an under-voltage state depends on the severity of the fault, which is identified as either a load-shed level 1 (LS1) or a load-shed level 2 (LS2) event. For LS1, all non-essential subsystems are powered off and the satellite starts to tumble and enters Safe Hold Mode (SHM). LS2 turns off all switchable powered subsystems along with the Computer and Data Handling subsystem (C&DH) and the transponders.

The voltage values at which the two load-shed levels are triggered are determined by the circuit's components and cannot be altered in flight. Table 2 shows the reference load-shed voltage levels for entry and exit conditions. The entry and exit voltages recorded during the only genuine load-shed event to date is also displayed (labeled LS1 2016).

Table 2. Load-shed thresholds levels

	Load-Shed 1 (V)	**LS1 2016 (V)**	**Load-Shed 2 (V)**
Entry	25.1	25.7	24.3
Exit	25.7	25.9	26.3

An important observation was made regarding the proximity of the entry and exit voltage levels for LS1. As the internal resistance of the battery increases, the associated instantaneous change in voltage becomes increasingly

significant (a more detailed explanation of this effect is provided in section 2). Fig. 3 below illustrates a hypothetical power-negative situation in which the battery suddenly becomes the only power source for the satellite. In this scenario the load-shed 1 threshold is eventually reached, and the non-essential components are shut down. From a typical 1.1 A draw, the discharge rate decreases to around 0.5 A due to the activation of LS1. With a high battery internal resistance of 2.0 Ω, this sudden change in power draw results in a nearly instantaneous voltage increase of 1.2 V (2.0 Ω × 0.6 A), bringing the voltage back into the nominal operating range, above the LS1 exit level. This situation can be problematic, as the load-shed flag signal would rapidly toggle and almost certainly not be recorded by the FSW. This would not give the operations team a direct explanation for why most subsystems were switched off simultaneously.

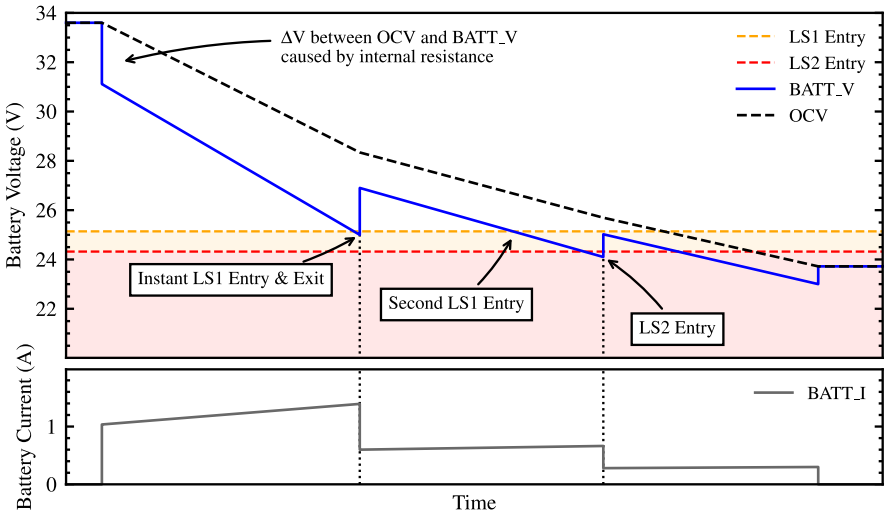

Fig. 3. Illustration of a power negative situation, with autonomous load-shed reactions

Still in a situation where the solar arrays are not producing power, the battery voltage would once again reach the LS1 entry threshold. By that time, however, all non-essential subsystems will have already been turned off, so the power draw remains unchanged. Consequently, the LS1 flag remains set long enough for the FSW to record it. Eventually, the voltage reaches the LS2 entry threshold. Because the gap between the LS2 entry and exit thresholds is relatively large, the load reduction from LS2 is insufficient to raise the voltage above the exit thresholds.

1.3.3 Power Budget

Table 3 below shows the maximum and average power consumption for each main subsystem. Note that the values for the Attitude Determination and Control system (ADCS) have been updated to account for current existing component failures (x-axis wheel, magnetometer and magnetorquers). The communications subsystem has the largest power consumption due to the transmitter unit, which however is only used during real-time contact with a ground station. Certain loads, such as the reaction wheels, can generate rapid and large inrush currents during transients, which may cause overshoots above the reported maximum power in Table 3. Due to the relatively slow data sampling rates, these spikes would not be detectable in telemetry but could still trigger a load-shed reaction.

Table 3. Power usage per subsystems under nominal operations conditions

Subsystem	Current Draw @ 33V (A)		Power Draw (W)	
	Maximum	Average	Maximum	Average
Communications	1.14	0.18	37.7	6.1
ADCS	0.65	0.32	21.5	10.5
Payload	0.40	0.30	13.2	10.0
PCDU	0.19	0.17	6.3	5.7
Onboard Computer	0.13	0.11	4.3	3.6
Thermal	0.05	0.03	1.5	0.9
TOTAL	**2.56**	**1.12**	**84.4**	**36.8**

2. METHODOLOGY

2.1 Internal Resistance Estimation

The internal resistance of a battery is a parameter that directly influences its power capability. It is well known that resistance varies with temperature, state of charge, and the overall state of health of the battery [2]. Because of its dynamic nature, assigning a unique value to the battery's internal resistance is quite challenging. It is highly dependent on the measurement conditions and the determination method, with this dependency being specific to each battery system. A lithium-ion battery's internal resistance can be evaluated by examining how its voltage changes in response to a step change in current. The resulting voltage drop arises from several resistance contributors, each occurring over different timescales [3]:

- Ohmic Resistance (R_0):
  - Results from the battery's materials resistance and the movement of ions in the electrolyte. The effect on the battery voltage is almost instantaneous and remains constant over time.
- Charge Transfer Resistance (R_{CT}):
  - This effect is due to the double-layer capacitance and charge transfer resistance at the electrode-electrolyte interface and decay exponentially over a few seconds before remaining constant.
- Diffusion Polarization Resistance (R_D):
  - Related to ion transport, this resistive component induces a nearly linear decrease. It often acts as the main bottleneck in lithium-ion batteries.

Studying these effects separately helps in understanding battery performance. Another factor influencing measured voltage is the natural tendency of a battery to lose potential as it discharges, which can be described using open-circuit voltage (OCV) versus state of charge (SoC) curves. For an active satellite in orbit, measurement techniques are often constrained by the limited ability to inject and control test signals. More advanced techniques, such as electrochemical impedance spectroscopy using AC current signals, cannot be applied to such systems. Additionally, the data sampling rate is often too low to capture rapid transient effects. Therefore, the methodology must rely on DC signals and longer-term regimes.

In [4], the authors describe a methodology for estimating battery resistance based on a so-called direct current resistance (DCR) parametrization. Using a DCR-based approach, the effects of diffusion polarization and OCV variations are largely eliminated for internal resistance estimation. This leads to a more accurate parameterization that primarily reflects ohmic resistance and charge transfer resistance. Since these two factors play a major role in the battery's dynamic power response within the relevant operating range, this method provides a reliable assessment of performance. Fig. 4 below shows a typical battery voltage response to a discharge pulse current, from a resting state with no active load. The different contributors to the voltage change are annotated, along with the DCR voltage drop (ΔV_{DCR}) used to evaluate the battery's internal resistance via Ohm's law:

$$R_i = \frac{\Delta V_{DCR}}{\Delta I_P}$$

Where R_i is the resulting battery internal resistance, and ΔI_p is the current pulse amplitude.

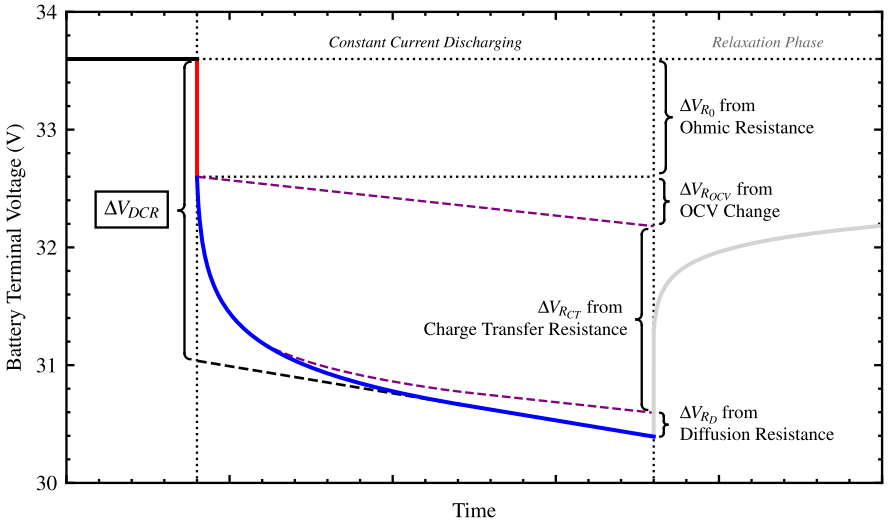

Fig. 4. Typical voltage curve during a constant current discharge with main contributors to voltage drop and ΔV_{DCR} estimation using linear fitting

The method illustrated in Fig. 4 is often referred as the current-injection approach. Another method called current-interruption can also be used in a similar fashion by removing the load completely or partially after the equilibrium state is reached. In most cases the current-interruption method gives a slightly lower resistance estimation compared to the current-injection method, the difference coming mainly from the diffusion polarization and the change of OCV [2]. In this analysis, only the current-interruption method will be used.

All estimations will be done using a simple graphical technique to find the best linear fit to the voltage curves. All estimations will be made using a simple graphical technique to find the best linear fit to the voltage curves. While this method is straightforward, it introduces uncertainties and subjective variations. However, given the overall accuracy of the data used and the numerous factors influencing internal resistance estimation, the precision of this technique is considered adequate for the study's purpose. This is true as long as the methodology and measurement parameters, such as temperature and initial state of charge, remain consistent throughout the analysis.

In Fig. 5, the current-injection method was applied using NEOSSat's battery voltage and current telemetry data to evaluate the voltage drop caused by the internal resistance.

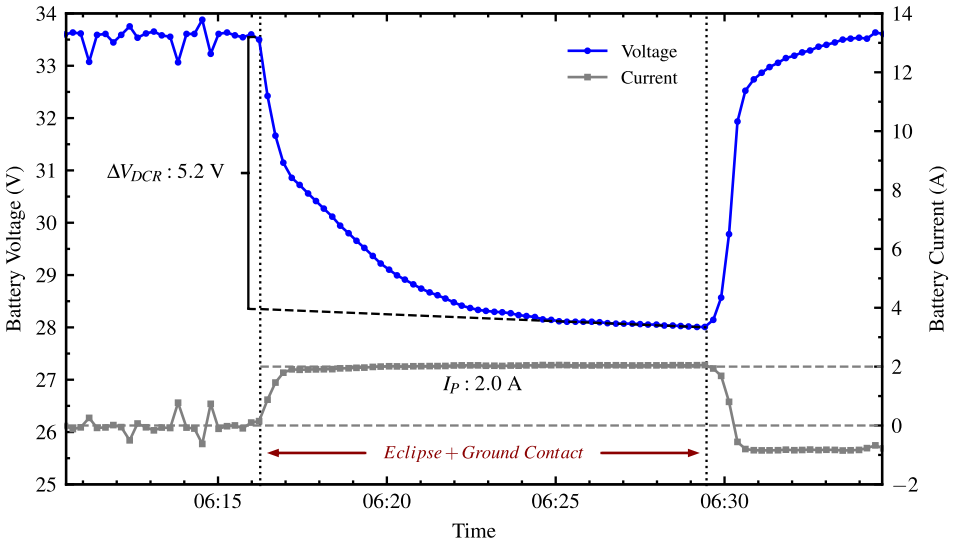

Fig. 5. Current-injection method from NEOSSat's telemetry for internal resistance estimation

In this example, the spacecraft entered an eclipse period at 06:16:15, causing the entire active load to switch to battery power. Around the same time, the transmitter was turned on for a scheduled ground contact and the total load increased from an almost zero-current equilibrium state to around 2.0 A. The current pulse amplitude is therefore ΔI_P = 2.0 A. Simultaneously, the measured battery voltage dropped rapidly, eventually reaching a near-linear discharge rate after about 10 minutes. By extrapolating the linear section, ΔV_{DCR} is set at 5.2 V. Note that in this example, the transmitter-off coincided with the end of eclipse transition. Using these estimated values, a calculation for the battery internal resistance is be done via Ohm's law:

$$R_i = \frac{\Delta V_{DCR}}{\Delta I_P}$$

$$R_i = \frac{5.2\ \text{V}}{2.0\ \text{A}}$$

$$R_i = 2.6\ \Omega$$

Thus, in this example the internal resistance is estimated at 2.6 Ω.

3. Results and Discussion

3.1 Power System Noticeable Events

This section presents battery voltage and temperature long-term data sets from the beginning of the mission up to March 2025. Note that the eclipse seasons will be identified with the year they ended in. For Fig. 6 and Fig. 7, each data point represents a single statistical value generated from data of one full orbit (maximum, minimum, average or standard deviation). In Fig. 6, the battery voltage orbital minima have been plotted using the battery voltage telemetry data. The red horizontal line corresponds to the 25.6 V threshold for load-shed level 1.

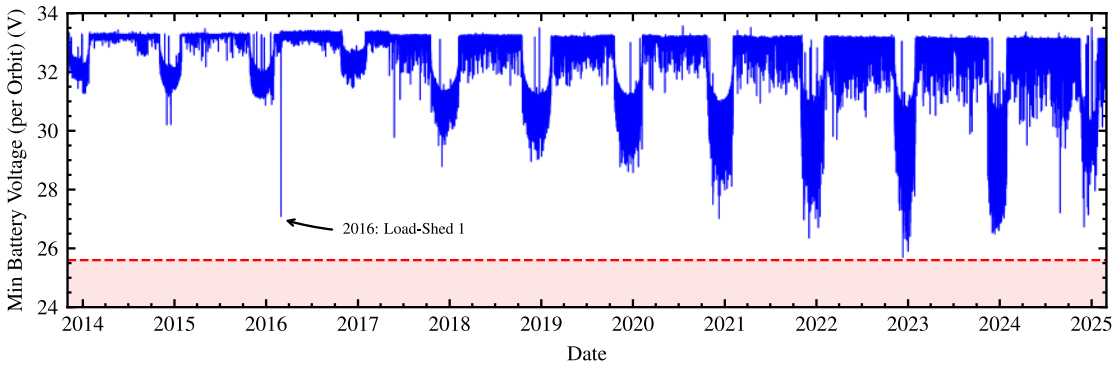

Fig. 6. Battery voltage (orbital minima) since the beginning of the mission

A slight downward trend is apparent during the first three eclipse seasons. However, the absolute minima during the 2017 season seem to report similar values as in the very first eclipse season. This is due to a change in baseline operations following the failure of both the magnetometer and the magnetorquer driver in 2016. The sudden magnetometer failure caused a loss of attitude control which had a harmful impact on the power system. Poor attitude determination and control prevented effective solar array pointing which eventually led to a level 1 load-shed reaction in early 2016. For the following eclipse seasons, the average minimum voltage maintained a decreasing trend, but with stabilization showing from season 2024.

Many factors influence the rate at which the battery system has degraded over time, including the operating temperature of the cells. NEOSSat's battery was designed to operate within a temperature range of 10 to 40 °C. Different temperature conditions result in different adverse effects, but operating the battery outside the recommended range always leads to a reduced efficiency, faster degradation rate and a higher risk of a permanent cell failure. In [5], a study evaluated the capacity fade of Sony 18650HC cells at temperatures ranging from 25°C to 55°C, with increasing numbers of 100% charge/discharge cycles. The results indicated that the rate of capacity fading doubled at temperatures above 45°C compared to 25°C, after 300 cycles or more. However, these test conditions differ significantly from NEOSSat's operational baseline, where the depth of discharge (DoD) is estimated to be only 5-10%, occurring solely during eclipse seasons.

In Fig. 7, the battery's average orbital battery temperature has been compiled. Again, the effect of the magnetometer failure on the battery temperature is clearly noticeable. Operational temperature limits are represented by the shaded area below 10 and above 40 °C.

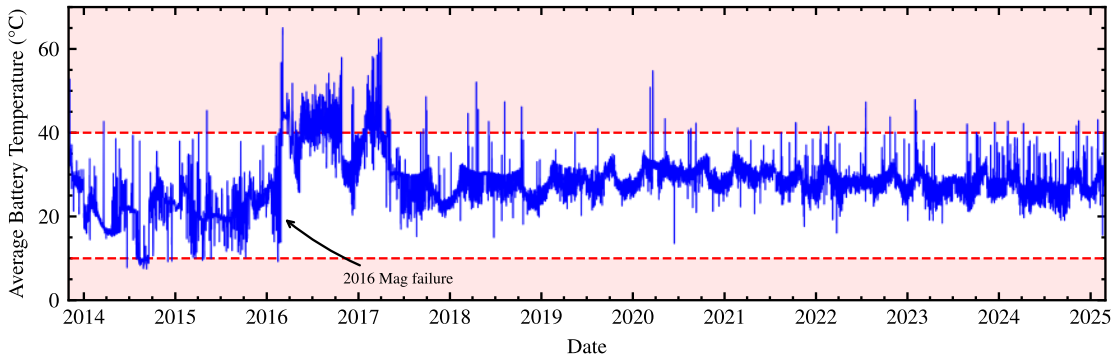

Fig. 7. Battery temperature (orbital average) since the beginning of the mission

Up until the activation of a new flight software with updated attitude algorithms to cope with the loss of the magnetometer and the torque rods in 2017, the battery was regularly operating around and above its maximum operational temperature. The long-term effects on the battery's health were difficult to evaluate at the time, but it is reasonable now to associate this high temperature phase with an accelerated increase of the battery internal resistance, as shown later in section 3.3.1. Subsequently, the battery temperature has been kept within its operational range, and maintained between 25 and 30 °C, with occasional spikes attributed to spacecraft anomalies.

3.2 Analysis of Load-Shed 1 Events of 2021-2022

In November of 2021, around one month after the eclipse season had started, NEOSSat's autonomous load-shed circuit triggered a level 1 load-shed in the middle of a real-time contact. This contact occurred while the satellite was in eclipse, with the battery as the only power source. The operations team identified an LS1 event based on the triggered command sequence and the resulting power-off states of the associated units, even though the load-shed flag was not set. Fig. 8 shows the battery voltage and current, along with the aggregated current draw of the reaction wheels around the time of the anomaly. A timeline of the events is as followed:

- 22:27:30 – The spacecraft enters Earth's shadow, and the power source switches to the battery
- 22:37:34 – The onboard transmitter is turned on for a real-time contact
- 22:41:40 – A time-tagged command triggered an attitude mode transition to Desat mode
- 22:42:22 – Multiple units are powered off by the load-shed circuit

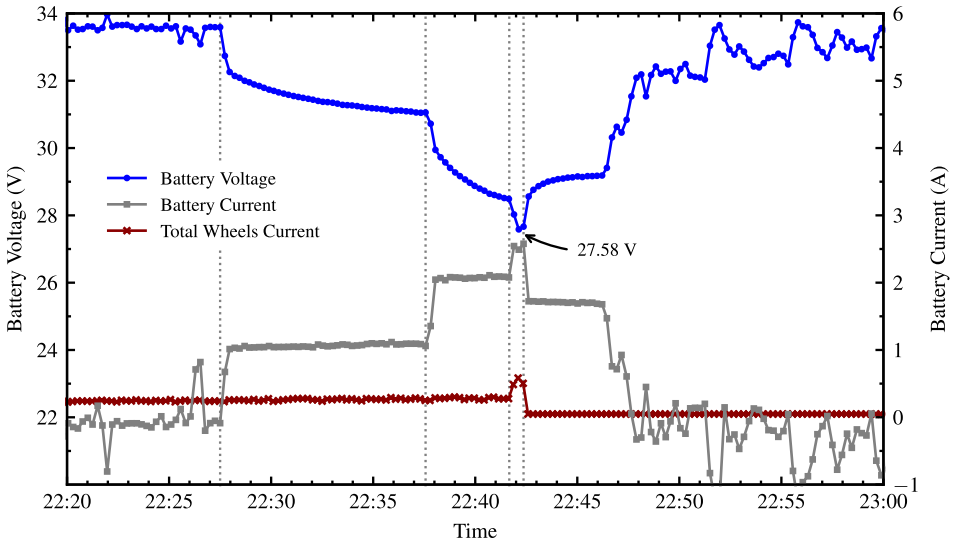

Fig. 8. Battery voltage, current and total wheels current around the first spurious LS1 in 2021

It was observed that the attitude mode transition at 22:41:40 generated large torque commands to the reaction wheels, resulting in sudden current demand on the battery.

The added load induced a voltage drop proportional to the battery resistance, which was large enough to trigger the LS1 reaction, even though the lowest recorded voltage remained around 2 V above the LS1 threshold, at 27.58 V. Note that voltage readings as low as 27.0 V had been observed previously without triggering a load-shed reaction. The relatively fast timescale of the current spike likely explains why the actual lowest voltage was not discerned. Moreover, as discussed in section 1.1.2, the rapid entry and exit from the load-shed range likely prevented the load-shed flag from being set and latched by the FSW.

Three other load-shed anomalies occurred during the 2021-2022 eclipse season, all under the same operational conditions:

- The spacecraft is in eclipse and powered by the battery.
- The transmitter is turned on for a real-time contact.
- An attitude mode transition to Desat mode occurs while the battery discharges at 2 A and the voltage drops below 28 V, but remains above the theoretical LS1 threshold.
- This is immediately followed by an autonomous load-shed level 1 response.

Following these events, a more thorough analysis was conducted throughout 2022 to better understand the issue and develop mitigation strategies for the upcoming eclipse season.

3.3 NEOSSAT's Power System State of Health Assessment Results

This section summarizes the main results and discussion points from the battery state of health analysis that was conducted in 2022.

3.3.1 Battery Internal Resistance Estimation

Fig. 9 presents the compiled results of battery internal resistance estimations. During each eclipse season, calculations were performed at multiple stages: around the first quarter, at the midpoint, and approximately three-quarters of the way through. The data points represent the average of all measurements taken throughout each eclipse season. For consistency, these points are aligned with January 1 of each year, which falls approximately two thirds of the way through the season. The error bars were computed using each dataset's standard deviation, with an additional subjective ±0.2 Ω to account for the combined uncertainty of the measurements and calculation method. The dataset spans two distinct phases, reflecting the change in operational baseline following the 2016 failures of the magnetometer and magnetorquers. During the one-year transition between these regimes, attitude control was precarious, making it difficult to keep thermally sensitive components out of direct sunlight. As a result, the battery was frequently exposed to elevated temperatures, often exceeding the operational limits.

Quantifying the battery degradation caused by the high-temperature phase is challenging, but it is reasonable to associate it with the increased rate of internal resistance growth observed between the 2017 and 2018 eclipse seasons.

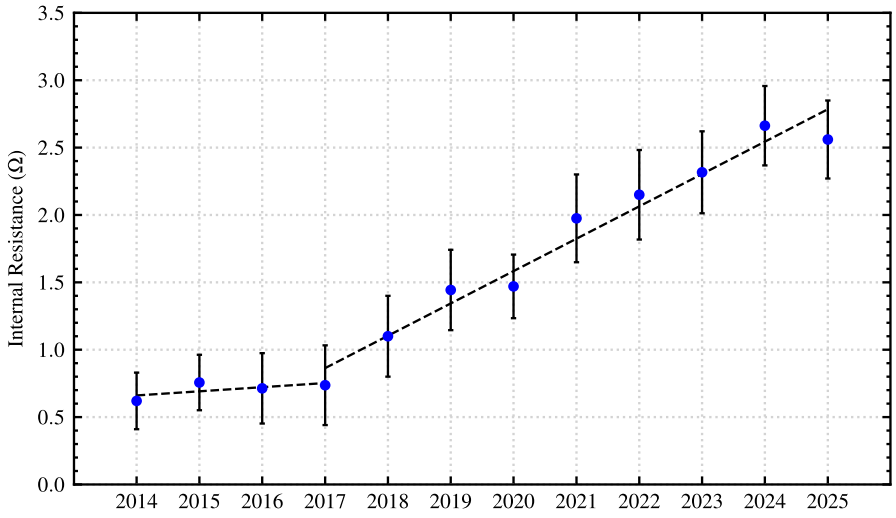

Fig. 9. Battery internal resistance estimation since launch

To characterize the dataset, linear fits have been applied to the graph in Fig. 9. Two separate linear trends are used for each operational phase. These regression fits will be used in the next section to project the future growth of the battery's internal resistance.

Fig. 10 shows representative battery voltage profiles at eclipse entry for each year of the analysis period. The datasets were selected under consistent operational conditions, including identical discharge current (nominal load with the transmitter off) and uniform battery temperature, to ensure comparability across years. The impact of the increasing internal resistance is readily apparent.

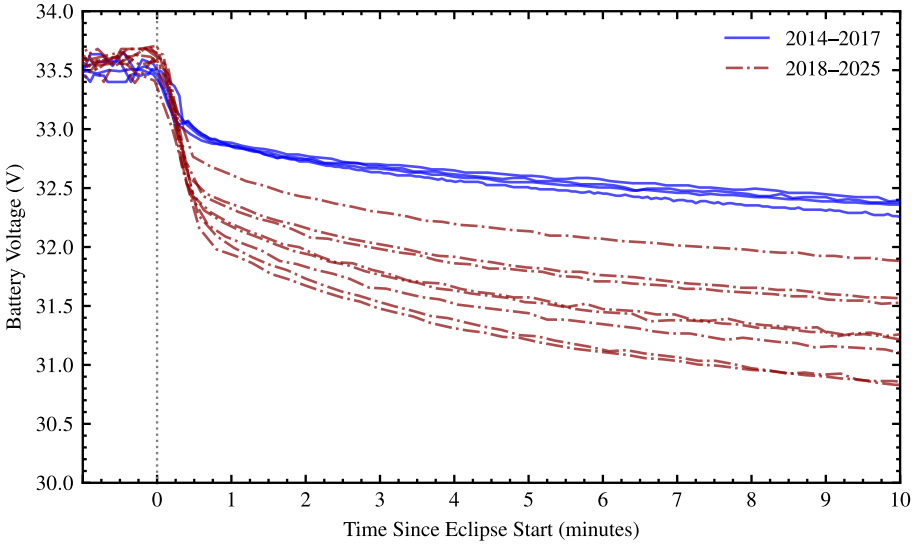

Fig. 10. Battery voltage at eclipse entry, with transmitter off

3.3.1.1 Projection of Future Battery Internal Resistance

On Fig. 11, the extrapolated trend line extends over the next eight years to estimate the future internal resistance increase and its effect. Shaded areas correspond to the LS1 and LS2 entry levels. For the last two eclipse seasons, the predicted values for the internal resistance were around 2.6 Ω. From a full charge, the effects of the internal resistance would pull the battery voltage from the nominal 33.6 V to around 28.4 V. The LS1 entry level being around 25.7 V (see Table 2), leaving no more than 2.7 V of headroom for ΔV_{OCV} and other potential disturbances on the bus before potentially triggering a LS1 event.

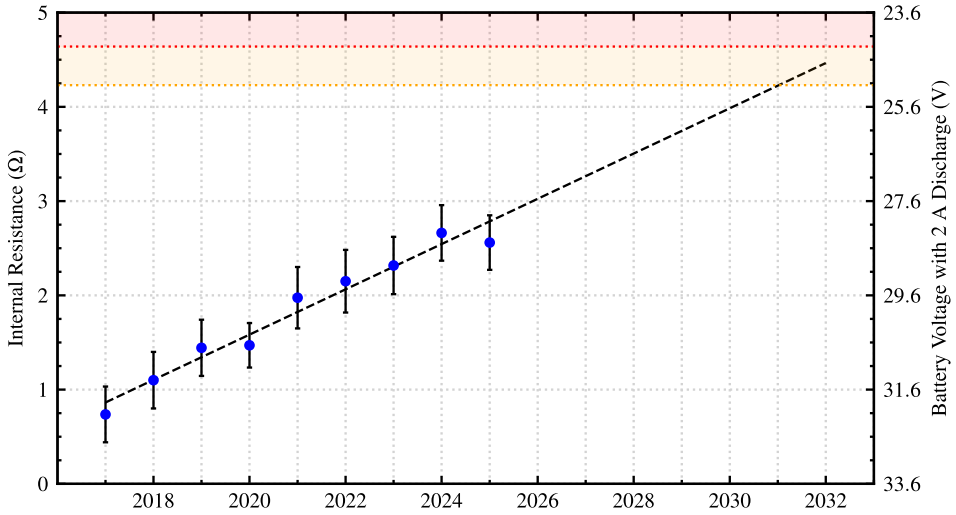

Fig. 11. Projected battery internal resistance

A similar analysis can be performed using the extrapolated predictions for the coming years. For season 2028-2029, the battery's internal resistance is estimated to reach up to 3.7 Ω, assuming current operational conditions remain unchanged and existing trends continue linearly. Using this worst-case approximation, it would translate into a rapid voltage drop from 33.6 V down to 26.2 V under a 2 A load during eclipse. This situation would be problematic and LS1 would almost certainly be triggered during a long eclipse period. It is important to note that the typical 2 A load seen from a full charge will increase as the voltage drops since the required power at the load remains nearly constant.

Consequently, 2.3 A would be required from the battery at a lower 26.2 V, exceeding the maximum recommended discharge rate of 2.25 A.

To illustrate this effect graphically, a plot of the load power against the battery discharge current is presented in Fig. 12. Each data series represents one fixed value of internal resistance, and the interception points with the different horizontal load lines indicate the associated current draw for a specific point of operation. For example, under the same power draw, the battery must deliver approximately 0.3 A more current in 2025 than it did in 2013.

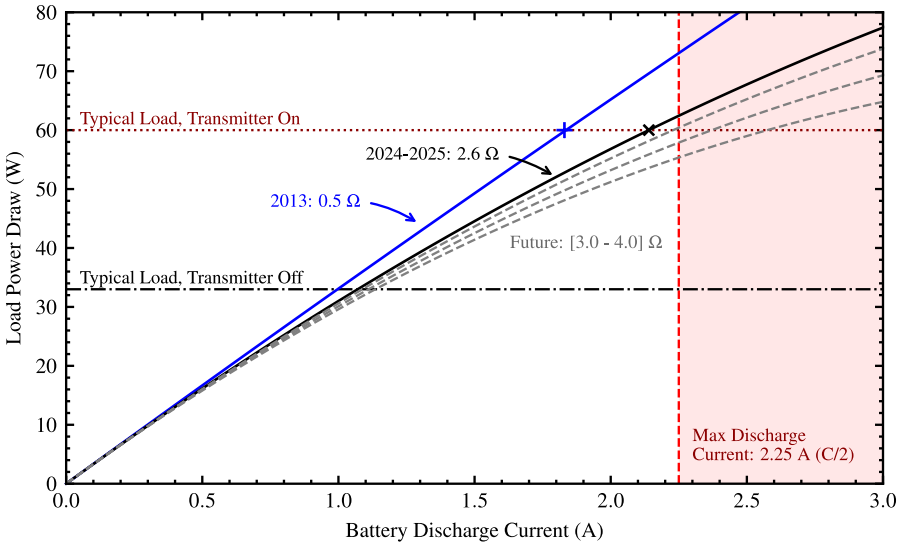

Fig. 12. Effect of the internal resistance increase on battery discharge current

3.3.2 Capacity Fade Examination

NEOSSat's battery was specified with a nominal 4.5 Ah total capacity. CSA performed a series of tests with the fully assembled spacecraft prior to launch in order to characterize the discharge/charge performance of the battery at that time. The test results were consistent with a total battery capacity of 4.4 Ah and a charging efficiency of 91%. The battery's capacity is expected to decline over time due to natural ageing.

No precise estimate of the projected battery capacity fading rate was found in the literature, but a long-term performance study on Sony 18650HC cells published in 2009 [6] offers relevant insights. One of the tests ran continuously for 7.5 years, during which two Sony 18650HC cells were cycled from full charge to an 18.75% Depth of Discharge (DoD) 32 times per day, totalling 73,567 charge cycles. In comparison, NEOSSat has so far been through roughly 11,440 charge cycles (1 cycle per orbit during eclipse season, 14.3 orbits per day, 100 days per eclipse season, 8 total eclipse seasons) and with estimated DoD of around 5 to 10%. A general conclusion from the study is that this type of cell could have endured many more charge cycles while still maintaining an end-of-charge voltage above the theoretical operational limit [6, p. 27]. Despite minor differences in environmental conditions and cell characteristics, this suggests that NEOSSat's battery should remain operational for many more cycles, and that it has likely retained most of its initial capacity.

Determining the battery capacity from telemetry data alone is challenging, as only a small fraction of the total capacity is used even during the longest eclipses, and the method depends on an accurate understanding of the battery's discharge curve to yield meaningful results.

Based on the method used in another CSA mission, a simple technique to estimate the capacity fade involves:

1. Identify a discharge period which begins from a full SoC and low current state
2. Collect battery voltage and current while discharging at a constant current
3. Calculate the V_{OCV} at the end of discharge by subtracting the voltage drop caused by the internal resistance
4. Integrate the current over time to get the total capacity used C_{used}
5. Lookup V_{OCV} in a known discharge table to determine an end-of-discharge State of Charge value, SoC_{OCV}
6. Calculate the new battery capacity C_{new} according to:

$$C_{new} = \frac{C_{used}}{1 - SoC_{OCV}}$$

For this method to produce conclusive results, a complete and precise discharge table is usually required. Many other factors such as divergence in cell degradation, imbalance between battery modules, and inaccuracies in internal resistance estimation also contribute to the problem. Several attempts were made to estimate the battery capacity fade using flight data and approximated discharge tables, but the resulting uncertainty was consistently too high to draw meaningful conclusions.

An indication that the battery retains sufficient capacity is the short recharging periods observed after each eclipse. A charging period is considered complete once the battery voltage stabilizes near its nominal value of 33.6 V and the charging current drops to minimal levels. Recent observations indicate that the battery consistently reaches full charge after a duration approximately equal to the preceding eclipse, a pattern that has remained unchanged since the beginning of the mission. This also suggests that the solar arrays continue to provide enough power to fully recharge the battery between eclipses.

3.4 Spurious Load-Shed Mitigation Strategy

For all load-shed events of 2021-2022, the attitude mode transition to Desat appears to have been the trigger. Mission planning ensures sufficient Desat periods to allow for continuous operations, and transitions to this mode are scheduled to maximize payload availability.

Before the 2023 eclipse season, a new feature was added to the mission planning constraints to detect conflicts between Desat transitions and scheduled ground station contacts during eclipses to better plan the avoidance of load-sheds. In its first iteration, the feature only flagged overlapping events, requiring manual intervention to adjust the schedule and shift the Desat transition. While effective, this process often demanded quick turnaround times from the operations team, especially when it impacted payload operations. As an additional preventive measure, the real-time contact procedure was modified to instruct the console operator to manually shut down the onboard transmitter if the battery voltage dropped below 27 V for at least two consecutive samples. These corrective actions proved effective during the 2023 eclipse season, with no spurious load-shed events recorded.

Prior to the 2024 season, the mission planning constraints was integrated into the user's scheduling process, which takes place upstream of spacecraft mission planning and outside the CSA operations center. This system update eliminated the need for the operations team to manually adjust the science schedule before uploads when a Desat transition was automatically inserted during an eclipse and a ground station contact.

Despite the implemented mitigation measures, three load-shed events were recorded during the 2024 eclipse season. While each anomaly had a similar signature, they differed from the events of 2021-2022. In all cases, the spurious load-shed occurred in eclipse while the spacecraft was transmitting to a ground station. However, unlike previous cases, no transition to Desat mode took place around the time of the fault. Instead, for all 2024 events, a known and recoverable ADCS anomaly was developing during the contact. By analysing the reaction wheels' power draw and commanded torque, the same underlying trigger as in 2022 was identified: rapid and large torque commands causing a sudden surge in battery current. Fig. 13 shows the battery voltage, the battery current and the total reaction wheels current during the first load-shed anomaly of the 2024 season.

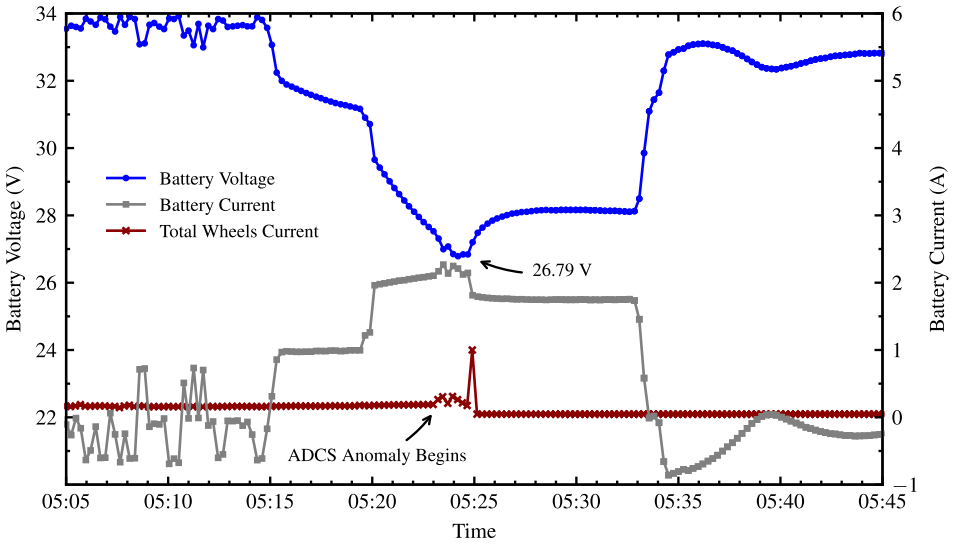

Fig. 13. Battery voltage, current and total wheels current around a spurious LS1 in 2023

The curves resemble those of the first spurious load-shed event from the 2022 season (Fig. 8), but with a steeper voltage decline due to the increased internal resistance. This effect also leads to a more pronounced current surge as the system compensates to maintain constant power delivery to the load, particularly between the transmitter-on command at 05:20 and the anomaly occurrence. The lowest recorded battery voltage, at 26.79 V, was lower than in the 2022 events but still more than 1 V above the highest known threshold reported in Table 2. For the two other incidents of 2024, the lowest reported battery voltages heading to the load-shed were 26.90 V and 26.23 V. Even if those were below the 27.0 V limit for a manual ground intervention, the on-console operator could not confirm the anomaly and react in time. With the increased battery internal resistance progressively amplifying the negative effects of high current draw, it became clear that additional preventive measures would be needed to ensure nominal operations in the future.

Further investigation was conducted during the non-eclipse period of 2024, leading to the proposal of additional mitigation strategies. To avoid using the transmitter in eclipse entirely, the option of utilizing an external ground station in the Southern Hemisphere was raised. Based on a partnership agreement between The German Aerospace Center (DLR) and CSA, DLR was contacted to explore the possibility of supporting NEOSSat's ground communication via their German Antarctic Receiving Station (GARS) during its eclipse season. The station had already supported NEOSSat's contacts during the early phases of the mission. Situated at 63.3° South latitude, this location would ensure that real-time operations always take place in full sunlight. After formal agreements were established, a series of tests were conducted before the 2025 eclipse season and GARS was ultimately designated as the primary ground station for NEOSSat contacts for the upcoming eclipse period. The Canadian ground stations continued to be used during periods of sunlight, when available. Shorter eclipses also provided more overall ground contact opportunities in sunlight. As shown in Fig. 1, eclipse durations peaked at 22 minutes in 2018–2019 and recently hit a low of 17 minutes. However, they are expected to increase again starting in 2026, reducing future contact opportunities over Canadian ground stations.

During the 2024-2025 eclipse season, only one spurious load-shed event occurred. The battery voltage and current around the event are shown on Fig. 14. It happened during a special recovery activity that required using a Canadian ground station, while the satellite was in eclipse for the entire duration of the pass. Unfortunately, a spurious load-shed level 1 was triggered during the recovery process, further delaying the ongoing payload outage.

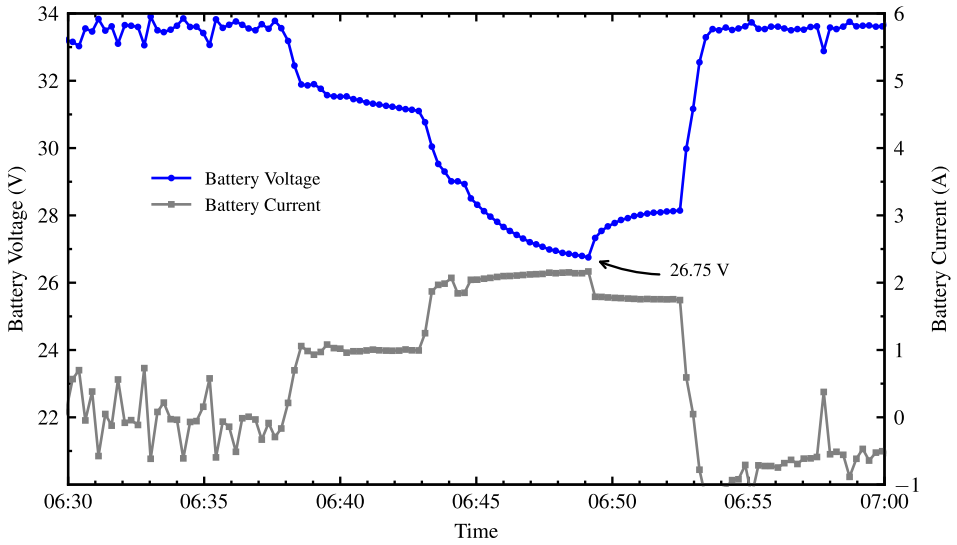

Fig. 14. Battery voltage and current during the load-shed event of season 2025

In this case, the lowest recorded voltage was 26.75 V. No significant disturbances were observed in the reaction wheels telemetry. Thus, this case can serve as a reasonable reference for estimating the actual LS1 threshold from battery voltage telemetry.

Also in 2024, part of the team began evaluating new reaction wheel controller gain designs to minimize the suspected inrush current caused by large torque commands. Implementing this update would require a new flight software version, which must be thoroughly tested before activation onboard. Initial tests shown promising results, and a formal development phase took place. As of the time this paper was written, however, the new flight software had not yet been uploaded to the satellite.

Another potential mitigation strategy involves developing a software-based load-shed strategy to replace the hardware LS1 reaction. As mentioned in section 1.3.2, NEOSSat's current load-shed mechanism is implemented through dedicated circuitry that directly acts on the PCDU, without any software intervention. While this approach is robust, it lacks flexibility for on-orbit adjustments. Nonetheless, a FSW approach could still be developed on top of the hardware method. In 2012, CSA outlined the requirements for such a software solution. These conditions are summarized here:

- A good correlation must be obtained between the OCV and the Amp-hour integrator methods to estimate the state of charge of the battery.
- The battery internal resistance and battery total capacity would need to be uploadable parameters in the software to allow compensating for aging of the battery or failure of a cell.
- The initial battery charge efficiency of 90% would also need to be an uploadable parameter for the same reasons.

Although the software could never fully override the load-shed circuitry (LS2 cannot be disabled), it could trigger an autonomous pre-emptive response to prevent an undesired load-shed event, while still preserving protection against genuine power-negative situations.

3.5 Contingency Case: Loss of One Battery Module

The failure of a battery cell would most likely cause a circuit interruption isolating a whole battery module from the circuit. In this situation, the battery would continue to operate at the same nominal voltage, but with a reduced total capacity and an increased resistance. Assuming uniform electrical characteristics across all cells, this corresponds to a 50% increase in internal resistance and a 33% decrease in total capacity, as shown from the equations below.

$$R_{2BM} = \left(\frac{1}{R_{i1}} + \frac{1}{R_{i2}}\right)^{-1} = 1.5 \cdot R_{3BM}$$

$$C_{2BM} = C_1 + C_2 = \frac{2}{3} \cdot C_{3BM}$$

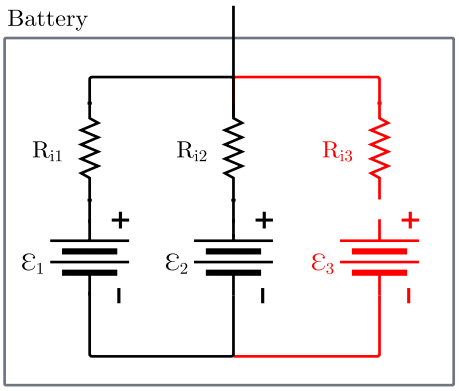

Fig. 15. Battery equivalent circuit with one failed module

Fig. 15 here shows the altered equivalent circuit. A more in-depth analysis would be advisable if such a situation were to occur. Nonetheless, it can be estimated that with the sudden increase in battery internal resistance, discharge current would likely rise above the maximum recommended value of C/2, which would now be equivalent to 1.5 A (2/3 of the nominal value with 3 active BM). The new operation baseline under a 60 W load would require around 2.6 A from the battery, as seen on Fig. 16. Nominal operations in eclipse but without real-time contacts would still be possible without exceeding C/2 discharge current. Using the latest internal resistance estimations, the degraded battery with only two remaining modules would then have an equivalent internal resistance of 3.9 Ω. Similarly, this increase would lead to lower voltage levels and thus increased risk of triggering an autonomous load-shed reaction.

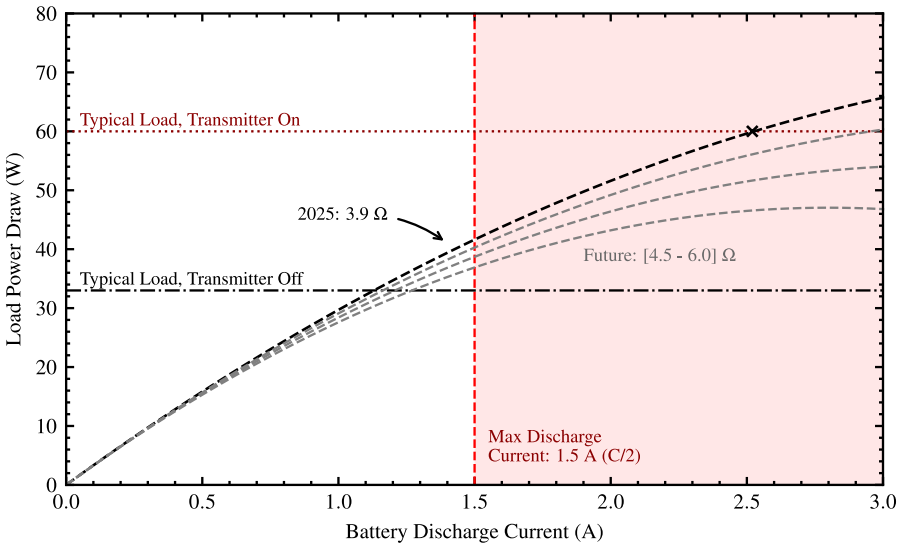

Fig. 16. Battery load curves with one failed module

4. CONCLUSION

After over 12 years of operations, NEOSSat's power system remains capable of generating sufficient energy and power to sustain nominal and continuous operations throughout the year. The capacity fade could not accurately be measured quantitatively, although there are many signs revealing that it is still generously above the minimum capacity required to sustain operations during the eclipse seasons.

One significant consequence of battery degradation is the marked increase of its internal resistance. Estimations indicate that the total internal resistance is currently around 2.6 Ω. A direct impact is evident during the annual eclipse season, when the satellite's power source is periodically switched to the battery each orbit. During these eclipse events,

the bus voltage drops to levels approaching the undervoltage thresholds and can cause spurious autonomous load-sheds, pausing all science operations until a manual recovery is complete. This issue first arose in 2021, prompting the operations team to implement various mitigation strategies to address the problem. The latest battery state-of-health assessment suggested a slowdown in its degradation. Negative effects of battery ageing are not reversible, but with the current mitigation measures in place, hazardous operating conditions can be completely avoided.

In the future, the operations team plans to implement additional mitigation measures through updated and new flight software features to better adapt the system to evolving constraints caused by battery degradation. Reaction wheel controller gains are being adjusted to minimize inrush current from sudden torque changes. Additionally, a software-based load-shedding mechanism could replace the current LS1 system, which is no longer well suited for this role. These enhancements will help ensure NEOSSat's continued operation, enabling it to adapt to the natural aging of its systems and extend its mission for many more years.

References

[1] V. Abbasi, N. Jackson, M. Doyon, R. Wessels, P. Sekhavat, M. Cannata, R. Gillett et S. Eagleson, NEOSSat Recovery Following Magnetometer and Torque Rod Failure, *2018 SpaceOps Conference*, 2018.

[2] B. Ratnakumar, M. Smart, L. Whitcanack et R. Ewell, The impedance characteristics of Mars Exploration Rover Li-ion batteries, *Journal of Power Sources*, vol. 159, 2, pp. 1428-1439, 2006.

[3] A. Barai, K. Uddin, W. D. Widanage, A. McGordon et P. Jennings, A study of the influence of measurement timescale on internal resistance characterisation methodologies for lithium-ion cells, *Scientific Reports*, vol. 8, 2018.

[4] J. V. Barreras, C. Pinto, R. d. Castrot, E. Schaltz, S. M., S. J. Andreasen et R. E. Araujo, An Improved Parametrization Method for Li-ion Linear Static Equivalent Circuit Battery Models Based on Direct Current Resistance Measurement, *International Conference on Sustainable Mobility Applications, Renewables and Technology (SMART)*, 2015.

[5] P. Ramadass, B. Haran, R. White et B. N. Popov, Capacity fade of Sony 18650 cells cycled at elevated temperatures Part I. Cycling performance, *Journal of Power Sources*, vol. 112, 2002.

[6] The Aerospace Corporation, Performance of SONY 18650 HC Lithium-Ion Cells for Various Cycling Rates, 2009.